



Electrochemical corrosion behaviour of Zn–Sn–Cu– x Ni lead-free solder alloys

Wen-jing CHEN¹, Nan YE², Hai-ou ZHUO², Jian-cheng TANG^{1,2}

1. School of Physics and Materials Science, Nanchang University, Nanchang 330031, China;

2. International Institute for Materials Innovation, Nanchang University, Nanchang 330031, China

Received 27 May 2022; accepted 1 September 2022

Abstract: Zn–30Sn–2Cu– x Ni ($x=0, 0.5, 1.0, 1.5$, wt.%) lead-free solder alloys were prepared via the casting method. Subsequently, their microstructures and corrosion behaviors in 0.5 mol/L NaCl solution were investigated. The electrochemical behaviour was studied using potentiodynamic polarization and electrochemical impedance spectroscopy (EIS) techniques, to evaluate the influence of Ni content on the corrosion performances of the Zn–Sn–Cu alloy. The corrosion mechanism of the Zn–Sn–Cu–Ni alloys was analyzed by observing surface structure evolution during the corrosion process. The results revealed that the addition of 0.5 wt.% Ni improved the corrosion resistance of Zn–30Sn–2Cu alloy due to forming a denser and more homogeneous corrosion layer, which acted as a physical barrier. The phase identification confirmed that the main corrosion products consisted of ZnO, Zn(OH)₂, and Zn₅(OH)₈Cl₂·H₂O. As the Ni content reached 1.0 and 1.5 wt.%, the corrosion resistance of Zn–30Sn–2Cu alloy declined, which could mainly be attributed to the galvanic corrosion between the (Ni,Cu)₅Zn₂₁ intermetallics and Zn-rich phase, accelerating the dissolution of Zn-rich phase. Thus, Zn–30Sn–2Cu–0.5Ni solder alloy showed the best corrosion resistance.

Key words: Zn–Sn–Cu–Ni alloy; microstructure; polarization; electrochemical impedance spectroscopy (EIS); galvanic corrosion

1 Introduction

The traditional Sn–Pb solder alloy, which causes environmental pollution and threatens human health, has gradually been replaced by lead-free solders [1–3]. Nowadays, Zn–Sn solder alloy is widely favored by researchers due to its superior strength, hardness, and cost-effectiveness [4]. However, since the activity of Zn leads to poor oxidation resistance, wettability, and corrosion resistance, the development of Zn–Sn solder alloy has been restricted in the field of electronic packaging. According to a previous study, adding multiple elements to Zn–Sn alloy is an effective strategy to address the above concerns [5].

So far, the family of Zn–Sn alloys has been

widely investigated. WANG et al [6] studied the corrosion behavior of Zn–20Sn alloy and found that its poor corrosion resistance could be attributed to severe galvanic corrosion between the Zn phase and Sn phase. Besides, the coarsened Zn with more defects resulted in high pitting susceptibility and poor electrochemical properties [7,8]. Therefore, considering the poor corrosion resistance exhibited by the Zn–Sn alloys, some researchers found that alloying methods could enhance the corrosion resistance of Zn–Sn alloys.

PEREIRA et al [9] reported that such methods could effectively enhance the corrosion resistance of Zn–Sn alloy. The addition of In improved the electrodeposition efficiency to form corrosion layers, which protected the alloy from corrosion. ZHANG et al [10] claimed that Sm alloying can

enhance the corrosion resistance of Zn–30Sn–Cu alloy and found that the Zn–30Sn–2Cu–0.5Sn alloy possesses a smaller corrosion current density and higher total resistance compared to Zn–30Sn–2Cu alloy. In addition, the effects of Ni alloying in improving the oxidation resistance and corrosion resistance of Sn–Zn alloy with appropriate Ni contents were extensively investigated [11–13]. Ni could react with Zn to form the stable $\text{Ni}_5\text{Zn}_{21}$ phase, thus, restricting the content of the active Zn element. Hence, the selective corrosion of alloys can be reduced, and the corrosion properties of Sn–9Zn– x Ni solders can be enhanced with the addition of Ni [14]. However, only a few studies have reported the enhanced corrosion resistance of Zn-based alloy with Ni addition. Besides, studies on the effects of Ni on the electrochemical behavior of Zn–Sn–Cu alloys are also scarce.

Thus, the current work aims to investigate the feasibility of designing Zn–Sn–Cu–Ni alloys as novel lead-free solder from the perspective of corrosion properties. Very few studies have determined the effect of Ni on the corrosion properties of Zn–Sn–Cu alloys. Therefore, Zn–30Sn–2Cu– x Ni ($x=0, 0.5, 1.0, \text{ and } 1.5, \text{ wt.}\%$) alloys were prepared, and the electrochemical behaviour was studied using potentiodynamic polarization and electrochemical impedance spectroscopy (EIS) techniques, to evaluate the influence of Ni on the corrosion performances of the Zn–Sn–Cu alloy. The corrosion mechanism of the Zn–Sn–Cu–Ni alloys was analyzed by observing surface structure evolution during the corrosion process using scanning electron microscope (SEM) and transmission electron microscope (TEM). The phase compositions of corrosion products were investigated by X-ray diffraction (XRD). The discussion is focused on the role of Ni on the corrosion performance.

2 Experimental

The Zn–30Sn–2Cu– x Ni alloys with $x=0, 0.5, 1.0$ and 1.5 (wt.%) were used in the current study. Pure Zn, Sn, Cu, and Cu–50Ni master alloys (purity higher than 99.99%) were used as the raw materials to prepare these samples. All metals were weighed according to the designed composition and melted in a graphite crucible at $(600\pm 5)^\circ\text{C}$ for 4 h. Then, these melted alloys were immediately transferred into a steel mold (preheated at 200°C) to form a cast alloy with a cross-section of $10\text{ mm} \times 10\text{ mm}$ and 10 mm in height. The chemical compositions of the Zn–30Sn–2Cu– x Ni alloys were determined using inductively coupled plasma atomic emission spectrometry (ICP-AES) and actual compositions are listed in Table 1.

The electrochemical measurements were performed using the CS305H electrochemical system (Corrtest Ltd., China) in 0.5 mol/L NaCl solution at room temperature. The electrochemical measurements were carried out in a traditional three-electrode system. The Zn–30Sn–2Cu– x Ni alloys were used as the working electrodes, Pt spiral wire as the counter electrode, and saturated calomel electrode with supersaturated KCl as the reference electrode. The surface of the working electrode was immersed in 0.5 mol/L NaCl solution. The electrochemical impedance spectroscopy (EIS) was used with an applied sinusoidal perturbation of 10 mV RMS (root-mean-square), corresponding to the open circuit potential (OCP), and the range of frequency was from 0.01 to 100000 Hz. The potential range was from -0.1 to 0.7 V , and the scan rate was set to be 0.5 mV/s . The experimental EIS and potentiodynamic polarization curves were analyzed using the ZVIEW and CS studio5 software, respectively.

The micro-morphologies of the as-cast alloys

Table 1 Chemical compositions of experimental Zn–30Sn–2Cu– x Ni alloys analyzed by inductively coupled plasma atomic emission spectroscopy (ICP-AES) (wt.%)

Alloy	Sn	Cu	Ni	Fe	Sb	As	Zn
Zn–30Sn–2Cu	30.05	1.95		0.010	0.02	0.009	Bal.
Zn–30Sn–2Cu–0.5Ni	30.11	2.03	0.52	0.012	0.02	0.008	Bal.
Zn–30Sn–2Cu–1.0Ni	29.93	2.08	0.94	0.010	0.03	0.010	Bal.
Zn–30Sn–2Cu–1.5Ni	29.89	1.93	1.55	0.012	0.02	0.012	Bal.

and corrosion products were observed using a scanning electron microscope (SEM) equipped with an energy dispersive X-ray (EDS). In addition, electron probe micro-analyzer (EPMA), transmission electron microscope (TEM), and X-ray diffraction (XRD) methods were used to determine the phase composition of sample alloys and corrosion products.

3 Results and discussion

3.1 Microstructure of Zn–30Sn–2Cu–*x*Ni alloys

Figure 1 exhibits the microstructures of Zn–30Sn–2Cu–*x*Ni solder alloys before electrochemical measurements. The microstructure of Zn–30Sn–2Cu alloy mainly consists of bright and dark areas. The bright area is the β -Sn phase, and the dark area is the α -Zn phase [15]. A typical eutectic structure is identified, in which the needle-like Zn-rich phases are distributed in the β -Sn phase, as shown in Fig. 1(a). The Zn-rich phases gradually transform from needle-like to spherical-like in Zn–30Sn–2Cu–0.5Ni alloy, as displayed in Fig. 1(b). This transformation is

associated with a reduction in the size of the Zn-rich phase. As the content of Ni increases to 1.0 and 1.5 wt.%, the finer spheroidal Zn-rich phases are detected, and they are more uniformly distributed within the β -Sn phase. Interestingly, a new phase is identified, as marked by the red circles in Figs. 1(c, d). According to the EDS results of S1 shown in Fig. 1(d), the new phase comprises of 13.39 at.% Ni and 7.45 at.% Cu and 79.16 at.% Zn, indicating that it is a Ni–Cu–Zn ternary compound. Furthermore, the amount of Ni–Cu–Zn ternary compounds gradually increases with an increase in the content of Ni.

Figure 2 depicts the EPMA mapping result of elements for the Zn–30Sn–2Cu alloy before electrochemical measurements. The result of element mapping confirms that the area with the high Cu concentration existed alongside the high Zn concentration area, indicating that the Cu–Zn binary compound is formed in the Zn–30Sn–2Cu alloy. As exhibited in Fig. 3, the mapping element for the Zn–30Sn–2Cu–1.5Ni alloy is slightly different from that shown in Fig. 2. From the results shown in Fig. 3, it can be noticed that Ni is

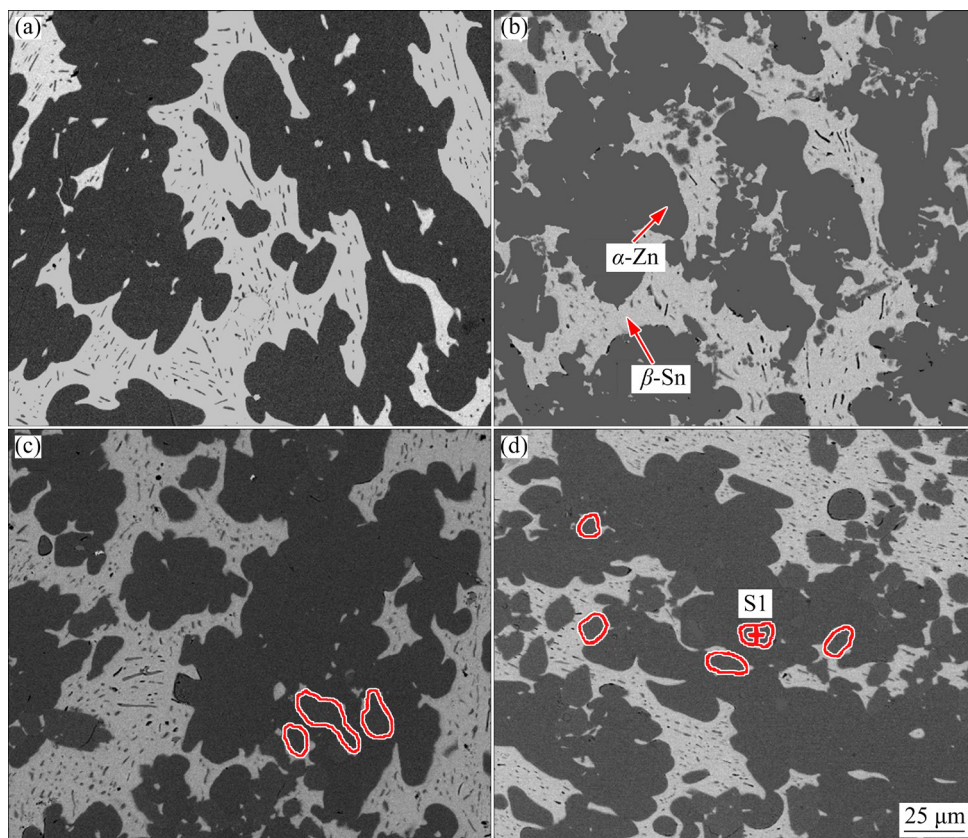


Fig. 1 BSE-SEM microstructures of Zn–30Sn–2Cu–*x*Ni alloys before electrochemical measurements: (a) Zn–30Sn–2Cu; (b) Zn–30Sn–2Cu–0.5Ni; (c) Zn–30Sn–2Cu–1.0Ni; (d) Zn–30Sn–2Cu–1.5Ni

concentrated in minor regions marked using red circles, in which both Cu and Zn are also detected. This suggests that the Ni–Cu–Zn ternary compounds are primarily present within these regions.

Figure 4 shows the TEM image and selected area diffraction (SAD) pattern for the Zn–30Sn–2Cu–1.5Ni alloy before electrochemical measurements. The selected area diffraction pattern

in Fig. 4(b) demonstrates that the crystal structure of the Grain A shown in Fig. 4(a) can be regarded as the body-centered cubic structure of the $\text{Ni}_5\text{Zn}_{21}$ compound (PDF 00-006-0635) [16]. Meanwhile, according to the results of EPMA in Fig. 3, the Cu element is present in the Ni–Cu–Zn ternary compound. This implies that part of Ni sublattices in the $\text{Ni}_5\text{Zn}_{21}$ crystal structure is replaced by Cu. Hence, Grain A can be identified to be $(\text{Ni,Cu})_5\text{Zn}_{21}$.

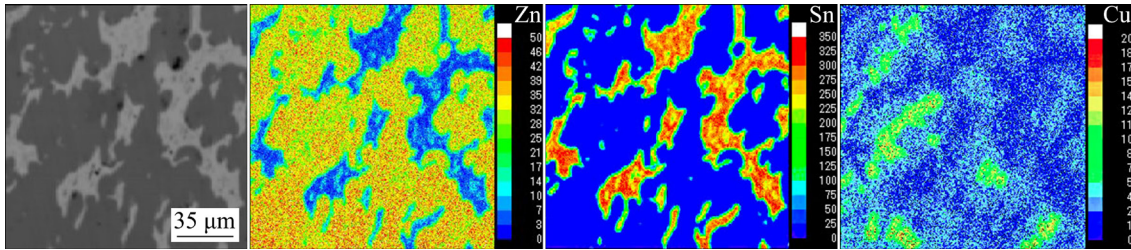


Fig. 2 EPMA mapping results of elemental distribution for Zn–30Sn–2Cu alloy before electrochemical measurements

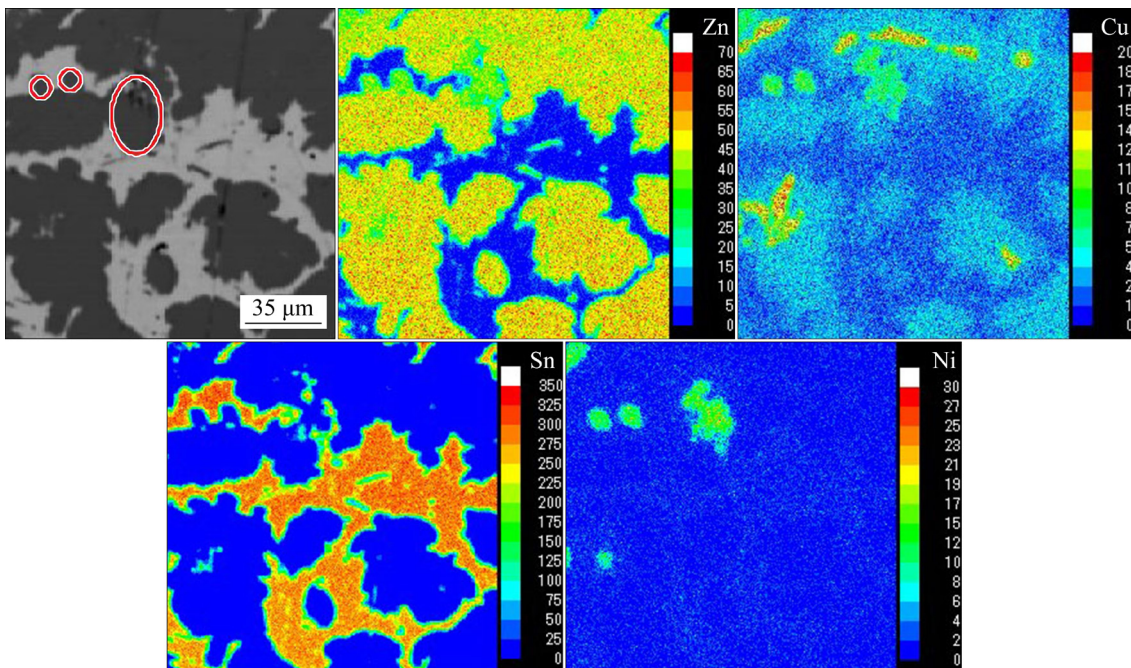


Fig. 3 EPMA mapping results of elemental distribution for Zn–30Sn–2Cu–1.5Ni alloy before electrochemical measurements

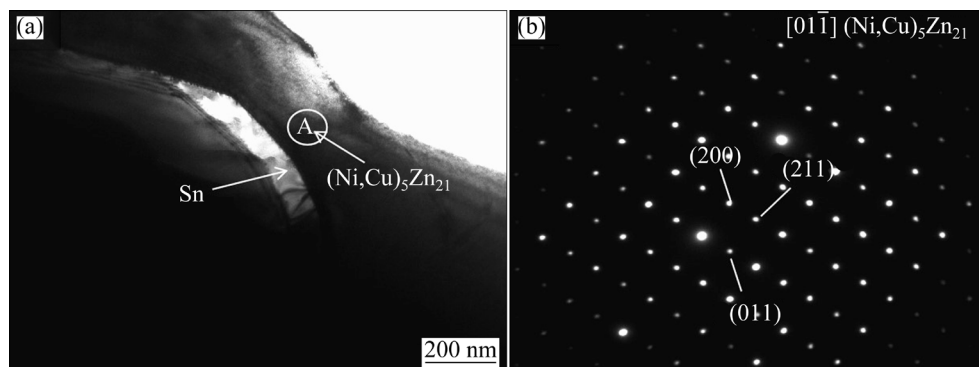


Fig. 4 TEM image (a) and SAD pattern (b) for Zn–30Sn–2Cu–1.5Ni alloy before electrochemical measurements

A similar phenomenon of Cu-doping in Ni_2Sn_3 IMC crystal structure was observed by CHENG et al [17].

3.2 Potentiodynamic polarization curves

Figure 5 shows potentiodynamic polarization curves of Zn–30Sn–2Cu– x Ni solder alloys, with $x=0, 0.5, 1.0,$ and 1.5 (wt.%) in 0.5 mol/L NaCl solution. The curves suggest that all the Zn–30Sn–2Cu– x Ni alloys have a similar polarization process. According to the polarization process, the corresponding corrosion process of these alloys can be regarded to be composed of three stages. The *AB* stage is a typical cathode polarization reaction with oxygen reduction in a neutral solution. WANG et al [6] reported a similar reaction on Zn–Sn alloys, which is described as

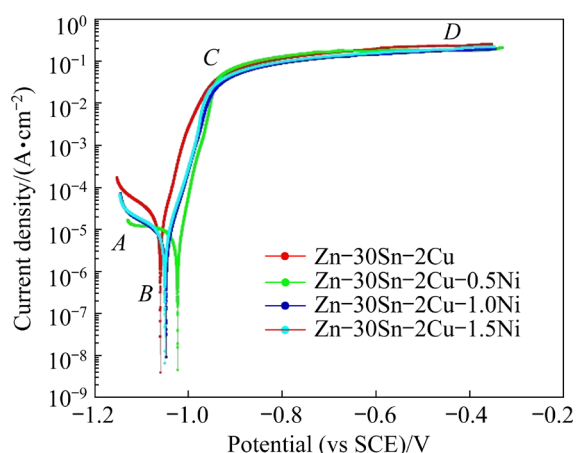


Fig. 5 Potentiodynamic polarization curves of Zn–30Sn–2Cu– x Ni ($x=0, 0.5, 1.0, 1.5$, wt.%) solder alloys in 0.5 mol/L NaCl solution

The further scanning of the anodic branch to the *BC* stage shows that the current density rapidly increases due to the dissolution of the Zn-rich phase for all alloys [12,18]. Until the potential reaches Point C, the concentration of active Zn serves as a critical value, and the current density is maintained

at about $0.1 \mu\text{A}/\text{cm}^2$. The main reason is that the corrosion product covers the surface of corroded alloys, which causes the development of a pseudo passivation film. This pseudo passivation film can hinder the movement of cathode ions through the surface of alloys and avoid further dissolution of the Zn-rich phase. According to LIU et al [19], passivation film formation leads to a rapid drop in the current density during the polarization process for the Sn–Zn alloys. In contrast, the pseudo passivation film does not result in a dramatic drop in the current density because such a pseudo film can only provide physical barrier protection for the alloys during the corrosion process.

The detailed parameters of potentiodynamic polarization curves are listed in Table 2. The corrosion current density (J_{corr}) is obtained by extrapolating from the cathodic Tafel region to the corrosion potential (φ_{corr}) due to the lack of clarity in the anodic Tafel region [20]. Data from Table 2 suggest that the value of corrosion potential (φ_{corr}) of Zn–30Sn–2Cu solder alloy was -1.059 V. This value is lower than that of the Zn–30Sn–2Cu– x Ni alloys ($x=0.5, 1.0, 1.5$), which are $-1.023, -1.047,$ and -1.051 V, respectively. In general, a lower value of φ_{corr} means more corrosion tendency thermodynamically. Thus, adding Ni can enhance the corrosion resistance of Zn–30Sn–2Cu alloys. Meanwhile, the corrosion current density of alloy varies dramatically with Ni addition. When the Ni content reaches 0.5 wt.%, the corrosion current density sharply declines from 16.19 to $5.66 \mu\text{A}/\text{cm}^2$. However, the corrosion current density slightly increases to 6.04 and $7.33 \mu\text{A}/\text{cm}^2$, respectively, as the Ni content reaches 1.0 wt.% and 1.5 wt.%. The significant difference in corrosion potential of the Zn-rich and $(\text{Ni,Cu})_5\text{Zn}_{21}$ phases would result in a reaction between the two phases, resulting in galvanic corrosion [6]. With the addition of Ni element, the primary Zn-rich phase gradually transforms into $(\text{Ni,Cu})_5\text{Zn}_{21}$ phase due to the

Table 2 Parameters of potentiodynamic polarization curves

Alloy	$b_c/(\text{mV} \cdot \text{decade}^{-1})$	$J_{\text{corr}}/(\mu\text{A} \cdot \text{cm}^{-2})$	$\varphi_{\text{corr}}(\text{vs SCE})/\text{V}$	Corrosion rate/ $(\text{mm} \cdot \text{a}^{-1})$
Zn–30Sn–2Cu	–105.9	16.19	–1.059	0.25515
Zn–30Sn–2Cu–0.5Ni	–144.1	5.66	–1.023	0.08808
Zn–30Sn–2Cu–1.0Ni	–123.1	6.04	–1.047	0.09238
Zn–30Sn–2Cu–1.5Ni	–130.8	7.33	–1.051	0.10988

b_c : Cathodic Tafel slope; J_{corr} : Corrosion current density; φ_{corr} : Corrosion potential

reaction between Ni and Zn. Due to the reduced Zn-rich phase, the ratio of cathodic area of $(\text{Ni,Cu})_5\text{Zn}_{21}$ to the anodic area of Zn-rich phase relatively increases. Based on the theory of galvanic corrosion [21], the higher ratio of cathodic area to the anodic area can lead to a faster dissolution rate of anodic alloy. Hence, the value of J_{corr} gradually increases with increasing Ni content. The Zn–30Sn–2Cu–0.5Ni alloy possesses the lowest corrosion current density value ($5.66 \mu\text{A}/\text{cm}^2$) among all considered solder alloys.

3.3 Electrochemical impedance spectroscopy

Figure 6 demonstrates the electrochemical impedance spectroscopy of Zn–30Sn–2Cu– x Ni ($x=0, 0.5, 1.0, 1.5, \text{wt.}\%$) solder alloys in 0.5 mol/L NaCl solution. From Nyquist plots (Fig. 6(a)), two capacitive arc radii are observed for all the alloys, suggesting their similar electrochemical properties. The lower capacitive arc radius can be related to the worse corrosion resistance [22]. Hence, the Zn–30Sn–2Cu–1.5Ni alloy has the worst corrosion

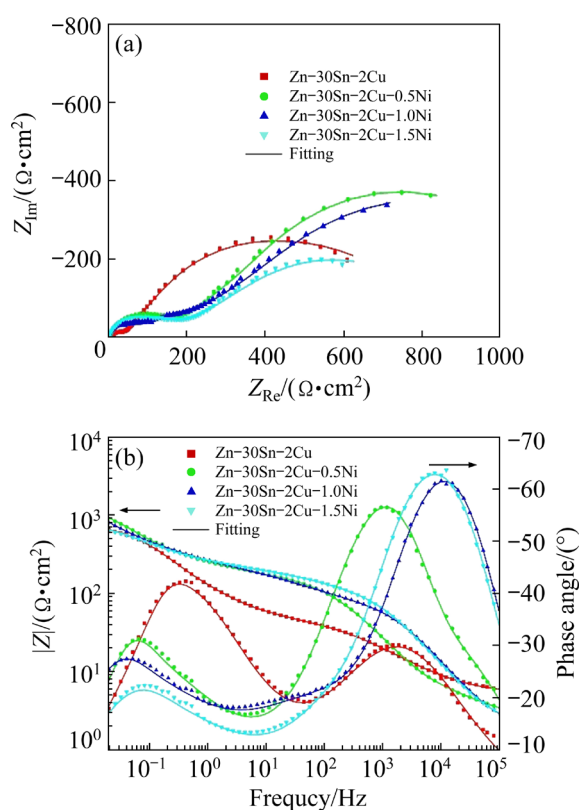


Fig. 6 Electrochemical impedance spectroscopy of Zn–30Sn–2Cu– x Ni ($x=0, 0.5, 1.0, 1.5, \text{wt.}\%$) alloys under their open-circuit potential after immersion in 0.5 mol/L NaCl solution for 90 min: (a) Nyquist plots; (b) Bode plots

resistance because of the lowest capacitive arc radius among all alloys. In addition, according to the bode plots in Fig. 6(b), two peaks appear in the range of 0.1–10000 Hz, indicating the existence of two time constants in the impedance spectra. Generally, the time constant at high frequency is associated with the interface reactions between the solution and the corrosion product layer [23]. Conversely, the time constant at low frequency is related to the double electrode layer between the surfaces of solder alloys and corrosion products. The Zn–30Sn–2Cu–0.5Ni alloy exhibits the highest $|Z|$ value at the low-frequency region, as shown in Fig. 6(b), corresponding to the longest semi-reactance arcs in Nyquist plots (Fig. 6(a)). It is noteworthy that these results are also in accord with the consequences of potentiodynamic polarization curves in Fig. 5.

Accordingly, an equivalent circuit was employed to fit the EIS data of Zn–30Sn–2Cu– x Ni alloys, as shown in Fig. 7. R_s is the solution resistance; R_1 and CPE_1 are, respectively, the resistance and capacitance of the corrosion product layer. R_2 and CPE_2 represent the charge transfer process and capacitance of the double electric layer between the interface of corrosion product and alloy, respectively. The constant phase element (CPE) for replacing the ideal capacitance is decided by looking at the distribution of surface reactivity, inhomogeneity, roughness, adsorption of species, and electrode porosity [19]. R_w represents the Warburg impedance to describe the concentration polarization process.

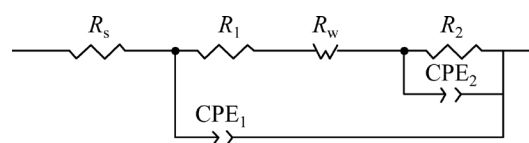


Fig. 7 Equivalent circuit (EC) model for EIS data fitting of Zn–30Sn–2Cu– x Ni ($x=0, 0.5, 1.0, 1.5, \text{wt.}\%$)

The fitting parameters of the equivalent circuit are given in Table 3. Standard deviation (λ^2) is used to represent the degree of fitting efficiency. In addition, a reasonable fitting standard with an error less than a magnitude of 10^{-4} is considered acceptable [24]. According to the data in Table 3, R_s values are slightly different for four kinds of solder alloys under the same experimental condition. The presence of charge transfer resistance (R_2) and

the Warburg impedance (R_w) confirms that the corrosion behavior of the alloys is controlled by the charge transfer process and concentration polarization process [25]. Moreover, the total resistance value (R_t), calculated as $R_t=R_1+R_2+R_w$, can be used to evaluate the corrosion resistance of the alloys [26]. The Zn–30Sn–2Cu–0.5Ni alloy possesses the highest value of R_t , 1397.3 $\Omega\cdot\text{cm}^2$, while the Zn–30Sn–2Cu alloy has the lowest value (853.8 $\Omega\cdot\text{cm}^2$). Hence, according to the EIS results, Zn–30Sn–2Cu–0.5Ni alloy exhibits the best corrosion resistance, while Zn–30Sn–2Cu alloy is the one with poor corrosion resistance.

3.4 Characterization of corrosion product

Figure 8 displays the SEM micrographs of the corrosion products on the surface of the alloys

after electrochemical measurements. As shown in Fig. 8(a), the corrosion product of Zn–30Sn–2Cu alloy possesses platelet-like morphology on the surface. WANG et al [27] observed a similar platelet-like morphology on the surface of Zn–30Sn alloy. With the increment of Ni contents, the platelet-like corrosion products gradually become denser and are more uniformly distributed on the surface, as evident from Figs. 8(b–d). However, it is worth noting that the obvious cavity structure is present on the corroded surface of both Zn–30Sn–2Cu–1.0Ni and Zn–30Sn–2Cu–1.5Ni alloys. It is indicated that the corrosion product film provides less physical barrier protection compared to that of Zn–30Sn–2Cu–0.5Ni alloy. The cavity structure can be considered as a transmission path for the penetration of anions to enter the interior of the

Table 3 Fitting parameters of equivalent circuit model

Solder alloy	$R_s/$ ($\Omega\cdot\text{cm}^2$)	$R_1/$ ($\Omega\cdot\text{cm}^2$)	CPE ₁		$R_2/$ ($\Omega\cdot\text{cm}^2$)	CPE ₂		$R_w/$ ($\Omega\cdot\text{cm}^2$)	$\lambda^2/$ 10^{-4}	$R_t/$ ($\Omega\cdot\text{cm}^2$)
			$Y_1/$ ($10^{-6}\Omega^{-1}\cdot\text{cm}^{-2}\cdot\text{s}^n$)	n_1		$Y_2/$ ($10^{-6}\Omega^{-1}\cdot\text{cm}^{-2}\cdot\text{s}^n$)	n_2			
Zn–30Sn– 2Cu	3.10	42.6	25.10	0.61	163.1	365	0.67	645	2.5	853.8
Zn–30Sn– 2Cu–0.5Ni	2.50	66.8	39.42	0.72	136.5	422	0.95	1254	6.3	1397.3
Zn–30Sn– 2Cu–1.0Ni	2.10	66.3	4.34	0.88	94.4	661	0.57	1117	1.6	1277.7
Zn–30Sn– 2Cu–1.5Ni	2.07	104.1	5.93	0.86	46.1	246	0.73	735	3.5	885.2

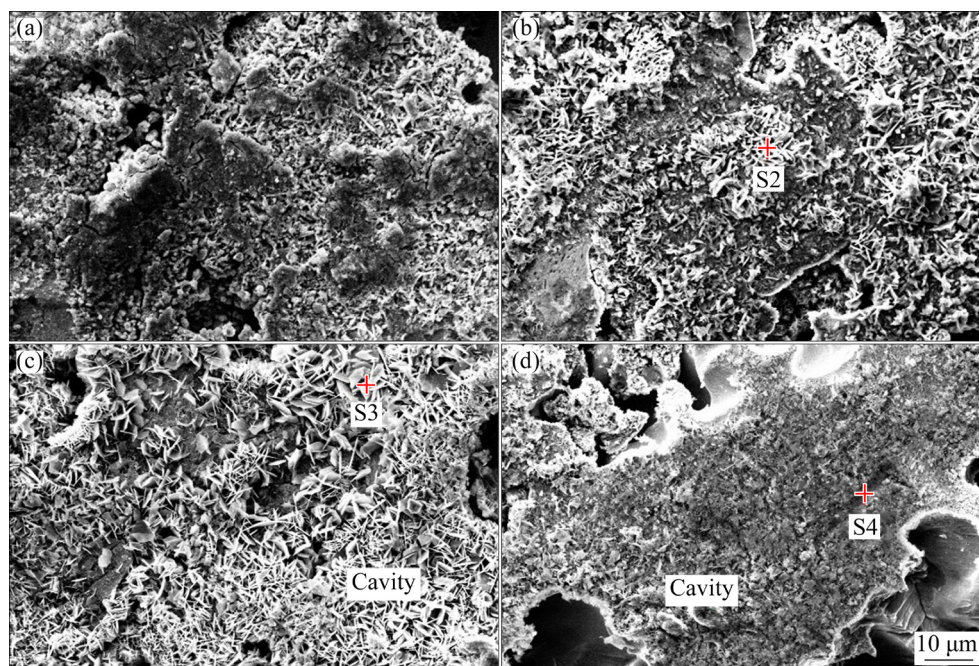


Fig. 8 SEM microstructures of Zn–30Sn–2Cu– x Ni alloys after electrochemical measurements: (a) Zn–30Sn–2Cu; (b) Zn–30Sn–2Cu–0.5Ni; (c) Zn–30Sn–2Cu–1.0Ni; (d) Zn–30Sn–2Cu–1.5Ni

alloy and for the corrosion products to reach the surface. This can lead to the further dissolution of the Zn-rich phase. As a result, the corrosion resistance of the alloy declines. LIU et al [19] also reported the role of a similar cavity on the corrosion resistance of Sn-*x*Zn solder alloys. Hence, the least cavity structure of Zn-30Sn-2Cu-0.5Ni alloy, among all considered alloys, might be a reason for its excellent corrosion resistance.

According to the EDS results of Zones S2 and S3 in Table 4, the platelet-like corrosion product is composed of high quantities of Zn and O, and low quantities of Sn and Cl, implying that the Zn-rich phase is primarily dissolved and depletes during the corrosion process. As demonstrated by the EDS analysis of Zone S4 (Table 4), the corrosion product on the surface of Zn-30Sn-2Cu-1.5Ni alloy is composed of minor Sn, Cl and Ni, and major Zn and O. This indicates that the (Ni,Cu)₅Zn₂₁ phase is not completely covered by the corrosion product. As shown in Fig. 1, the Zn-rich phase gradually changes from needle-like to spherical-like with the addition of Ni. LIU et al [28] reported that the corrosion products composed of spherical particles were porous, and their corrosion products were looser compared to the needle-like particles, which cannot provide good protection to the alloy substrate and therefore cannot completely cover the alloy surface. Thus, it does not get completely corroded. It can also explain why the corrosion product on the (Ni,Cu)₅Zn₂₁ phase is sparse.

Table 4 EDS analysis results of corrosion products marked in Fig. 8 (at.%)

Zone	Zn	Cl	O	Sn	Ni
S2	33.67	8.64	53.89	3.80	–
S3	33.86	9.05	56.69	0.39	–
S4	41.80	3.40	47.21	3.79	3.81

The XRD patterns are analyzed to further confirm the phase composition of corrosion products after electrochemical measurements (Fig. 9). It is revealed that a considerable quantity of the Sn phase remains, and the Zn-rich phase is nearly absent after corrosion, which is in agreement with the EDS results (Table 4). The result proves that the Zn-rich phase is preferentially corroded over the Sn phase. In contrast, the (Ni,Cu)₅Zn₂₁ intermetallic (IMC) is hard to get corroded because

of its relatively higher corrosion potential. In addition, the dominant corrosion products are composed of complex Zn hydroxyl chloride hydrate and related Zn compounds, namely Zn₅(OH)₈Cl₂·H₂O, Zn(OH)₂, and ZnO. This is consistent with the previous conclusion reported by LIU et al [29]. However, the corrosion products containing Sn are not detected from the XRD results shown in Fig. 9, indicating that the Sn-rich phase is relatively not corroded during the corrosion process. It is deduced that the corrosion potential of the Sn-rich phase may be higher than that of the (Ni,Cu)₅Zn₂₁ phase. Otherwise, the current effect should also occur between the Sn-rich phase and the (Ni,Cu)₅Zn₂₁ phase, which will aggravate the corrosion of the Sn-rich phase to form corrosion products mainly containing Sn. Meanwhile, the (Ni,Cu)₅Zn₂₁ phase and Ni₅Zn₂₁ phase have similar electronic structures, and WANG and LI [12] reported that Ni₅Zn₂₁ and β-Sn can exist stably at the interface at the same time without forming a new phase, so the corrosion potential of the Sn-rich phase may be higher than that of the (Ni,Cu)₅Zn₂₁ phase.

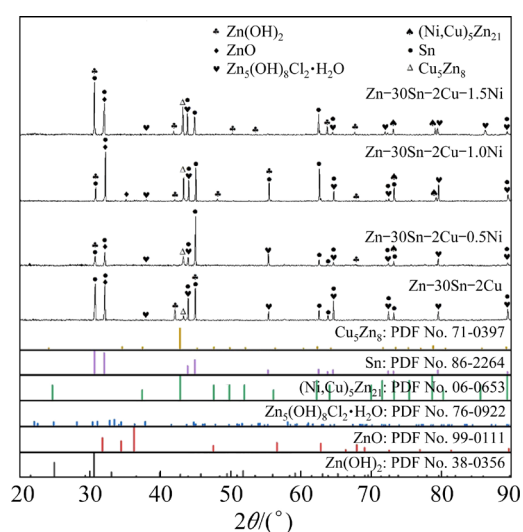


Fig. 9 XRD patterns of corrosion products formed on surface of Zn-30Sn-2Cu-*x*Ni alloys after electrochemical measurements in 0.5 mol/L NaCl solution

3.5 Discussion

Figure 10 displays the cross-sectional SEM morphology and mapping of elements of Zn-30Sn-2Cu-1.0Ni alloy after the electrochemical measurements. The mapping of elements in Fig. 10 shows that the Sn phase remains while the Zn-rich phase disappears from the top half part of the cross-section. It can be concluded that the Zn-rich

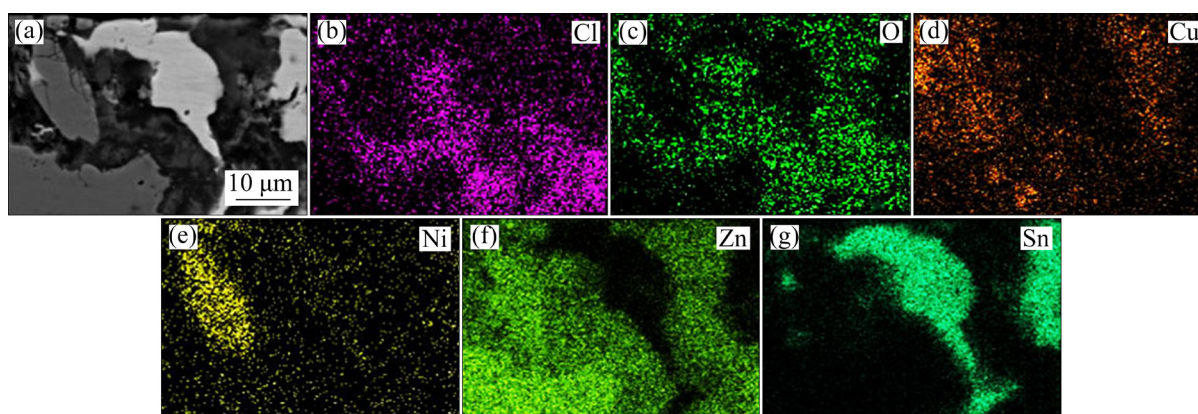


Fig. 10 SEM microstructure of cross-section (a) and mappings of distribution of elements (b–g) for Zn–30Sn–2Cu–1.0Ni alloy after electrochemical measurements in 0.5 mol/L NaCl solution

phase is selectively corroded. Meanwhile, Cl^- and OH^- are detected in the corrosion areas according to the results of elements mapping of Cl and O (Fig. 10). Those anions penetrate the interface between the corrosion product and alloy, resulting in the further corrosion of the inner Zn-rich matrix [23]. Interestingly, the Cu and Zn elements are also detected within the area of high Ni concentration, while the Cl and O elements are detected in an area surrounding it. Combining Fig. 1(c) and Fig. 10, it can be revealed that the Zn-rich phase around $(\text{Ni,Cu})_5\text{Zn}_{21}$ IMC is depleted, while the $(\text{Ni,Cu})_5\text{Zn}_{21}$ IMC does not get corroded. This phenomenon confirms the occurrence of galvanic corrosion between $(\text{Ni,Cu})_5\text{Zn}_{21}$ IMC and the Zn-rich phase.

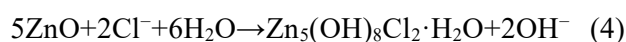
The main corrosion process could be divided into two stages. The first stage was the dissolution of Zn to form ZnO and $\text{Zn}(\text{OH})_2$. The reaction equations are as follows:



During this stage, the Zn-rich phase in Zn–30Sn–2Cu– x Ni alloys is selectively corroded, and remaining Sn phase is focused on the cathodic location. The O_2 and H_2O react with the Zn-rich phase, resulting in formations of the coarse zinc hydroxide and zinc oxide on the surface of alloys, causing the phase to corrode.

During the second stage, Cl^- and OH^- could permeate through the interface between the corrosion product and the surface of the Zn–30Sn–2Cu– x Ni alloys [6,27], causing the corrosion reaction at a certain depth in the alloys.

As a result, it would weaken the physical protection barrier of the corrosion product layer. During the process, a part of zinc oxide would be transformed into the insoluble zinc hydroxy chloride ($\text{Zn}_5(\text{OH})_8\text{Cl}_2 \cdot \text{H}_2\text{O}$). The reaction equation is as follows:



Accordingly, the corrosion products mainly consist of ZnO, $\text{Zn}(\text{OH})_2$, and $\text{Zn}_5(\text{OH})_8\text{Cl}_2 \cdot \text{H}_2\text{O}$. The result is also confirmed using the XRD data shown in Fig. 9.

When Ni is added to the Zn–30Sn–2Cu alloys, the needle-like Zn-rich phase gradually transforms into a spherical phase, as shown in Fig. 1. This results in the formation of a denser and more homogeneous corrosion product layer during the corrosion process, as shown in Fig. 8. The corrosion product layer provides a physical barrier to hinder the further dissolution of the Zn-rich phase. However, the increased amount of Ni addition (1.0 and 1.5 wt.%) to the Zn–30Sn–2Cu alloy leads to the formation of $(\text{Ni,Cu})_5\text{Zn}_{21}$ IMCs, which plays a significant role in weakening the corrosion resistance of alloys. The galvanic corrosion between $(\text{Ni,Cu})_5\text{Zn}_{21}$ and the Zn-rich phase occurs due to the lower chemical activity of the former in comparison to the latter. This, in turn, results in an accelerated dissolution of the Zn-rich phase [12]. Subsequently, the corrosion resistance of the Zn–30Sn–2Cu–1.0Ni and Zn–30Sn–2Cu–1.5Ni alloys weakens.

Generally, on the brighter side, the addition of Ni element to the Zn–Sn–Cu solder alloys can modify the morphology and distribution of the

Zn-rich phase and be beneficial for the formation of denser and more homogeneous corrosion products during the corrosion process. On the other hand, as the Ni content increases to 1.0 wt.% or more, the galvanic corrosion between the $(\text{Ni,Cu})_5\text{Zn}_{21}$ and Zn-rich phase accelerates gradually, resulting in a high dissolution rate of the Zn-rich phase and thereby weakening the corrosion resistance of the solder alloy.

4 Conclusions

(1) The addition of Ni element significantly influences the morphology of the Zn-rich phase, which transforms from coarser platelet-like morphology into a finer spherical shape. The finer Zn-rich phase reduces the corrosion susceptibility of the Zn–30Sn–2Cu alloy due to the formation of a denser and more homogeneous corrosion product on the surface of the alloy during the corrosion process.

(2) The potentiodynamic polarization results reveal that the Zn–30Sn–2Cu–0.5Ni alloy possesses the lowest corrosion current density. It can also be noted that the alloy exhibits pseudo passivation behavior during the corrosion process. EIS analysis illustrates that the total resistance is improved from 853.8 to 1397.3 $\Omega\cdot\text{cm}^2$ when 0.5 wt.% Ni is added to the Zn–30Sn–2Cu alloy. As a result, the resultant Zn–30Sn–2Cu–0.5Ni alloy displays the best corrosion resistance among all the studied alloys.

(3) For the Zn–30Sn–2Cu– x Ni alloys, the corrosion resistance gradually weakens when the Ni content reaches 1.0 wt.% or more, which can mainly be attributed to the galvanic corrosion between the $(\text{Ni,Cu})_5\text{Zn}_{21}$ IMCs and Zn-rich phase, resulting in the accelerated dissolution of Zn-rich phase.

Acknowledgments

The authors are grateful for the financial supports from the National Natural Science Foundation of China (No. 51864034).

References

[1] WANG Hao-zhong, HU Xiao-wu, JIANG Xiong-xin. Effects of Ni modified MWCNTs on the microstructural evolution and shear strength of Sn–3.0Ag–0.5Cu composite solder joints [J]. *Materials Characterization*, 2020, 163: 110287.

[2] QIAO Yuan-yuan, MA Hai-tao, YU Feng-yun. Quasi-in-situ observation on diffusion anisotropy dominated asymmetrical growth of Cu–Sn IMCs under temperature gradient [J]. *Acta Materialia*, 2021, 217: 117168.

[3] BI Xiao-yang, HU Xiao-wu, LI Qing-lin. Effect of Co addition into Ni film on shear strength of solder/Ni/Cu system: Experimental and theoretical investigations [J]. *Materials Science and Engineering A*, 2020, 788: 139589.

[4] SONG Jenn-ming, LIN Meng-ju, HSIEH Kun-hung, PAI Tsung-yun, LAI Yi-shao, CHIU Ying-ta. Ball impact reliability of Zn–Sn high-temperature solder joints bonded with different substrates [J]. *Journal of Electronic Materials*, 2013, 42: 2813–2821.

[5] GUO Wei-ting, LIANG Chien-lung, LIN Kwang-lung. The effects of Cu alloying on the microstructure and mechanical properties of Zn–25Sn– x Cu ($x=0-1.0$ wt.%) high temperature Pb-free solders [J]. *Materials Science and Engineering A*, 2019, 750: 117–124.

[6] WANG Zheng-hong, CHEN Chuan-tong, JIU Jin-ting, NAGAO S, NOGI M, KOGA H, ZHANG Hao, ZHANG Gong, SUGANUMA K. Electrochemical behavior of Zn– x Sn high-temperature solder alloys in 0.5 M NaCl solution [J]. *Journal of Alloys and Compounds*, 2017, 716: 231–239.

[7] EFZAN M, KAMANEEYA R. Corrosion of Sn–Zn–Bi lead free solder in KOH electrolyte [J]. *Solid State Phenomena*, 2018, 273: 51–55.

[8] LIU Jian-chun, ZHANG Gong. Effect of trace Mn modification on the microstructure and corrosion behavior of Sn–9Zn solder alloy [J]. *Materials and Corrosion*, 2018, 69: 781–792.

[9] PEREIRA J, SANTOS L, ALCANFOR A, CAMPOS O, CASCIANO P, CORREIA A, LIMA-NETO P. Electrochemical corrosion evaluation of new Zn–Sn–In coatings electrodeposited in a eutectic mixture containing choline chloride and ethylene glycol [J]. *Electrochimica Acta*, 2022, 407: 139647.

[10] ZHANG Hua-jin, HU Xiao-wu, LIU Yi, ZHANG Jian-kang, JIANG Xiong-xin, LI Qing-lin. Enhanced mechanical properties and corrosion behavior of Zn–30Sn–2Cu high-temperature lead-free solder alloy by adding Sm [J]. *Journal of Materials Science: Materials in Electronics*, 2022, 33: 6469–6484.

[11] WANG Chao-hong, CHEN Hsien-hsin. Study of the effects of Zn content on the interfacial reactions between Sn–Zn solders and Ni substrates at 250 °C [J]. *Journal of Electronic Materials*, 2010, 39: 2375–2381.

[12] WANG Chao-hong, LI Po-yi. Microstructure evolution of $\text{Ni}_5\text{Zn}_{21}$ intermetallic compound at Sn–9wt.%Zn/Ni interface [J]. *Materials Chemistry and Physics*, 2013, 138: 937–943.

[13] JING Yan-xia, SHENG Guang-min, HUANG Zhen-hua, ZHAO Guo-ji. Effects of 0.1 wt.% Ni addition and rapid solidification process on Sn–9Zn solder [J]. *Journal of Materials Science: Materials in Electronics*, 2013, 24: 4868–4872.

[14] HUANG M L, KANG N, ZHOU Q, HUANG Y Z. Effect of Ni content on mechanical properties and corrosion behavior of Al/Sn–9Zn– x Ni/Cu Joints [J]. *Journal of Materials Science and Technology*, 2012, 28: 844–852.

- [15] LIN Jeng-chi, LIANG Chien-lung, LIN Kwang-lung. Joint effects of Ti and Cu additions on microstructure and mechanical properties of Zn-25Sn-xCu-yTi high-temperature Pb-free solders [J]. *Materials Science and Engineering A*, 2019, 765: 138323.
- [16] ABEDINI B, PARVINI AHMADI N, YAZDANI S, MAGAGNIN L. Electrodeposition and corrosion behavior of Zn-Ni-Mn alloy coatings deposited from alkaline solution [J]. *Transactions of Nonferrous Metals Society of China*, 2020, 30: 548–558.
- [17] CHENG Jin-xuan, HU Xiao-wu, LI Qing-lin. Effects of the Ni electrodeposit on microstructure evolution and electrical resistance of the P-type Bi₂Te₃ solder joint [J]. *Journal of Alloys and Compounds*, 2020, 832: 155006.
- [18] NAZERI M, MOHAMAD A. Corrosion resistance of ternary Sn-9Zn-xIn solder joint in alkaline solution [J]. *Journal of Alloys and Compounds*, 2016, 661: 516–525.
- [19] LIU Jian-chun, PARK S, NAGAO S, NOGI M, KOGA H, MA Ju-sheng, ZHANG Gong, SUGANUMA K. The role of Zn precipitates and Cl⁻ anions in pitting corrosion of Sn-Zn solder alloy [J]. *Corrosion Science*, 2015, 92: 263–271.
- [20] PENG Xiang, SUN Jia-wei, LIU Hong-jie, WU Guo-hua, LIU Wen-cai. Microstructure and corrosion behavior of as-homogenized and as-extruded Mg-xLi-3Al-2Zn-0.5Y alloys (x=4, 8, 12) [J]. *Transactions of Nonferrous Metals Society of China*, 2022, 32: 134–146.
- [21] YANG Wen-lu, LIU Ze-qi, HUANG Hua-liang. Galvanic corrosion behavior between AZ91D magnesium alloy and copper in distilled water [J]. *Corrosion Science*, 2021, 188: 10956.
- [22] JIANG Qiong, MIAO Qiang, LIANG Wen-ping, YING Feng, TONG Fei, XU Yi, REN Bei-lei, YAO Zheng-jun, ZHANG Ping-ze. Corrosion behavior of arc sprayed Al-Zn-Si-RE coatings on mild steel in 3.5 wt.% NaCl solution [J]. *Electrochimica Acta*, 2014, 115: 644–656.
- [23] LIU Jian-chun, ZHANG Gong, WANG Zheng-hong, XIE Jing-yang, MA Ju-sheng, SUGANUMA K. Electrochemical behavior of Sn-xZn lead-free solders in aerated NaCl solution [C]//16th International Conference on (ICEPT) Electronic Packaging Technology. IEEE, 2015: 68–73.
- [24] CHAUDHARI S, CAIKWAD A, PATIL P. Synthesis and corrosion protection aspects of poly (o-toluidine)/CdO nanoparticle composite coatings on mild steel [J]. *Journal of Coatings Technology and Research*, 2009, 7(1): 119–129.
- [25] LIU Jian-Chun, ZHANG Gong, MA Ju-sheng, SUGANUMA K. Ti addition to enhance corrosion resistance of Sn-Zn solder alloy by tailoring microstructure [J]. *Journal of Alloys and Compounds* 2015, 644: 113–118.
- [26] OSORIO W, FEITOSA E, SPINELLI J, GARCIA A. Electrochemical behavior of a lead-free Sn-Cu solder alloy in NaCl solution [J]. *Corrosion Science*, 2014, 80: 71–81.
- [27] WANG Zheng-hong, CHEN Chuan-tong, LIU Jian-chun, ZHANG Gong, SUGANUMA K. Corrosion mechanism of Zn-30Sn high-temperature, lead-free solder in neutral NaCl solution [J]. *Corrosion Science*, 2018, 140: 40–50.
- [28] LIU Jian-chun, WANG Zheng-hong, XIE Jing-yang, MA Ju-sheng, SHI Qing-yu, ZHANG Gong, SUGANUMA K. Effects of intermetallic-forming element additions on microstructure and corrosion behavior of Sn-Zn solder alloys [J]. *Corrosion Science*, 2016, 112: 150–159.
- [29] LIU Guang-yu, KHORSAND S, JI Shou-xun. Electrochemical corrosion behaviour of Sn-Zn-xBi alloys used for miniature detonating cords [J]. *Journal of Materials Science and Technology*, 2019, 35: 1618–1628.

Zn-Sn-Cu-xNi 无铅焊料合金的电化学腐蚀行为

陈文静¹, 叶楠², 卓海鸥², 唐建成^{1,2}

1. 南昌大学 物理与材料学院, 南昌 330031;

2. 南昌大学 国际材料创新研究院, 南昌 330031

摘要: 通过铸造法制备 Zn-30Sn-2Cu-xNi (x=0, 0.5, 1.0, 1.5, 质量分数, %)无铅焊料合金, 并研究该合金的微观组织演化及在 0.5 mol/L NaCl 溶液中的腐蚀行为。采用电位动力学极化和电化学阻抗谱(EIS)技术研究其电化学行为, 以此评估 Ni 元素含量对 Zn-Sn-Cu 合金腐蚀性能的影响。通过观察腐蚀过程中合金表面显微组织的演变, 分析 Zn-Sn-Cu-Ni 合金的腐蚀机理。结果表明, 添加 0.5% Ni 由于形成致密而均匀的腐蚀层从而有效提高 Zn-30Sn-2Cu 合金的耐腐蚀性能, 且其主要腐蚀产物为 ZnO, Zn(OH)₂ 和 Zn₅(OH)₈Cl₂·H₂O。当 Ni 含量达到 1.0% 和 1.5% 时, Zn-30Sn-2Cu 合金的耐腐蚀性能下降, 主要是由于 (Ni,Cu)₅Zn₂₁ 金属间化合物与富 Zn 相之间的电偶腐蚀加速富 Zn 相的溶解。因此, Zn-30Sn-2Cu-0.5Ni 焊料合金具有最佳的耐腐蚀性能。

关键词: Zn-Sn-Cu-Ni 合金; 显微组织; 极化; 电化学阻抗谱; 电偶腐蚀

(Edited by Bing YANG)